

Article

Photobiological Effects on Ice Algae of a Rapid Whole-Fjord Loss of Snow Cover during Spring Growth in Kangerlussuaq, a West Greenland Fjord

Brian K. Sorrell ^{1,*} , Ian Hawes ² , Tanja Stratmann ^{3,4}  and Lars Chresten Lund-Hansen ¹

- ¹ Arctic Research Centre, Department of Biology, Aarhus University, Aarhus C., DK-8000 Aarhus, Denmark; lund-hansen@bio.au.dk
- ² Coastal Marine Field Station, Environmental Research Institute, University of Waikato, Sulphur Point, Tauranga 3110, New Zealand; ian.hawes@waikato.ac.nz
- ³ Department of Earth Sciences, Utrecht University, 3584 CB Utrecht, The Netherlands; tanja.stratmann@nioz.nl
- ⁴ HGF MPG Joint Research Group for Deep-Sea Ecology and Technology, Max Planck Institute for Marine Microbiology, 28359 Bremen, The Netherlands
- * Correspondence: brian.sorrell@bio.au.dk

Abstract: Snow cover on sea ice is the most important factor controlling light availability for sea ice algae, but it is predicted by climate models to become more variable and stochastic. Here, we document effects of a sudden, complete loss of the entire snow cover on first-year sea ice at Kangerlussuaq Fjord, West Greenland, due to a natural Föhn wind event that caused a ca. 17 °C air temperature increase over 36 h. We applied Imaging-PAM fluorometry to examine effects of snow cover on algal distribution and photobiology and observed a rapid decrease in algal biomass associated with loss of the skeletal ice crystal layer on the underside of the ice that had supported most of the visible algae. Furthermore, the remaining algae were photobiologically stressed, as seen in a significant decrease in the dark-acclimated fluorescence yield (Φ_{PSII_max}) from 0.55 before snow loss to 0.41 after. However, recovery in the dark suggested that non-photosynthetic quenching was successfully dissipating excess energy in the community and that there was little photodamage. An observed decrease in the photosynthetic efficiency α from 0.22 to 0.16 $\mu\text{mol } \epsilon \text{ m}^{-2} \text{ s}^{-1}$ is therefore likely to be due to photoacclimation and the change in community composition. Centric diatoms and flagellates were the main taxa lost in the snow loss event, whereas the sea ice specialist *Nitzschia frigida* increased in numbers. These observations are similar to those seen in artificial snow-clearing experiments and consistent with snow clearing being a useful approach for investigating the complex interactions between snow cover, irradiance fluctuations, and ice algal performance.



Citation: Sorrell, B.K.; Hawes, I.; Stratmann, T.; Lund-Hansen, L.C. Photobiological Effects on Ice Algae of a Rapid Whole-Fjord Loss of Snow Cover during Spring Growth in Kangerlussuaq, a West Greenland Fjord. *J. Mar. Sci. Eng.* **2021**, *9*, 814. <https://doi.org/10.3390/jmse9080814>

Academic Editor: Sang Heon Lee

Received: 31 May 2021

Accepted: 22 July 2021

Published: 27 July 2021

Publisher's Note: MDPI stays neutral with regard to jurisdictional claims in published maps and institutional affiliations.



Copyright: © 2021 by the authors. Licensee MDPI, Basel, Switzerland. This article is an open access article distributed under the terms and conditions of the Creative Commons Attribution (CC BY) license (<https://creativecommons.org/licenses/by/4.0/>).

Keywords: ice algae; Greenland; optics; photobiology; snow cover; stress

1. Introduction

Primary production in seasonally ice-covered polar oceans is driven by ice-associated and planktonic algae. While the proportional contributions of these two communities to primary production is variable [1], there is widespread support for the view that ice algae represent a significant source of carbon, not least because they are available in early spring before ice break-up allows planktonic algae to develop [2,3]. Although sea ice productivity often decreases greatly after spring, the remaining biomass persists throughout the season and continues to provide carbon to food webs well into the autumn [3,4]. The timing and flux of carbon flow during this process is an important coupling in the Arctic marine ecosystem [5]. In recent years, climatic warming has reduced the thickness and area of Arctic sea ice, which has led to concerns over the impacts of shifting patterns of primary productivity on Arctic ecosystems [6,7]. Sea ice algal biomass is generally dominated by diatoms concentrated at the ice–water interface [8,9], and these cells become available to seed phytoplankton [10] and to support higher trophic levels either by grazing within the

ice matrix or when they are released to the water column [1]. The timing of such release of ice algae to the water column is potentially significant, as it may change how and when other organisms can exploit the ice algae food resource [11] and when seeding of spring phytoplankton growth occurs [10].

Snow cover is a key variable affecting sea ice algae biomass and photosynthetic parameters but can have complex effects. Small reductions in thick snow cover can enhance ice algal accumulation, but rapid reduction in snow cover often results in equally rapid loss of ice algae [12]. Loss of algal biomass following sudden snow loss can be both physical, due to increased basal ablation increasing loss rates, and biological, through photoinhibition reducing growth [13,14]. Biomass can also fall after sudden increases in irradiance due to emigration of motile taxa, including flagellates and many pennate diatoms [14]. The amount of light transmitted through the snow–ice matrix and the ability of algal photobiology to acclimate to sudden changes in light intensity over different time scales are therefore critical to understanding increases, decreases, and losses of algal biomass in response to a changing Arctic snow cover.

Climate modelling has predicted both increased and decreased thicknesses of snow cover in the Arctic Ocean [15]; warmer air temperatures may make the coverage period much shorter, and the snow cover more dynamic with more frequent, sudden snow loss events. Most recent modelling suggests increased precipitation but less snow accumulation and more rainfall as the atmosphere warms [16]. There is considerable evidence of general declines in the duration of the snow-covered period in the Eurasian Arctic [17–19]; thus understanding the responses of ice algae to rapid shifts in snow cover has therefore become more important to understanding possible trajectories of change in the Arctic. At the local scale, however, snow trajectories are highly variable spatially and there is considerable inter-annual variability. For any given site, it is therefore important to compare responses across a range of snow thicknesses and hence irradiance scenarios to develop a complete insight into whether algal biomass is likely to change in response to broader climatic changes.

There are generally two approaches for studying effects of snowmelt on the ice algae community: first, manipulative field experiments involving complete or partial artificial snow removal, following effects from a subsequent time series [12,20], and second, measurement of selected parameters such as biomass or primary production as a function of natural variation in snow depth over space or time [21–23]. The limitations of these two approaches for understanding large-scale, rapid increases in irradiance in response to sudden snowmelt are evident. For logistical reasons, most snow-clearing experiments can only treat relatively small areas (a few square metres) and are not accompanied by realistic changes in air and sea ice temperatures during weather events, and therefore they may not accurately mimic whole-ecosystem algal responses during snowmelt events. Natural gradients, on the other hand, allow algae to acclimate to the prevailing irradiance and do not provide the sudden photoinhibitory stress driven by rapid snowmelt. Regrettably, researchers have few opportunities to study photobiological responses to snowmelt during the large-scale snowmelt events that sea ice algae often experience in nature.

In this paper, we are able to present a fortuitous account of a sudden weather-driven warming and large-scale snow loss event impacting an ice algal community on an entire fjord during the spring growth season at Kangerlussuaq, a Greenland fjord. This is, to the authors' knowledge, the first study of its kind, addressing the photobiological consequences of a rapid, wholesale natural loss of the snow cover over an entire fjord system. This type of event—sudden warming, with rainfall precipitation reducing snow cover—is very specifically a prediction of the most recent climate modelling [16]. In addition, there are still relatively limited data in the literature on in situ photosynthesis–irradiance parameters describing acclimation to under-ice irradiance, even though these are important in most current models relating ice algal biomass to snow cover and sea ice properties [24,25]. The specific objectives were therefore to study the effects on the photophysiology of ice algae following sudden snow loss, as well as the role of a ca. 17 °C air temperature increase within 36 h.

2. Materials and Methods

2.1. Site Description and Sampling Design

Our observations were made from 12 to 19 March 2013 at $66^{\circ}56.780\text{ N}$; $50^{\circ}52.853\text{ W}$, in Kangerlussuaq (Figure 1), a 180 km long, narrow (1–5 km) Arctic fjord located on the Arctic Circle on the west coast of Greenland, about 25 km from the Greenland ice sheet. It consists of a relatively shallow (30 to 40 m depth) outer part that connects with the open ocean and a deep-water inner part with depths up to 280 m [26]. Water depth at the sampling site was ca. 130 m. The tide is diurnal with a maximum tidal range of about 2–4 m [27]. The area has a continental climate with low average winter temperatures of -15 to $-25\text{ }^{\circ}\text{C}$ and low precipitation of ca. 5 mm per month during December–July (www.dmi.dk (accessed on 1 July 2021)). The fjord is ice-covered between October and early June to a thickness of about 0.5–1.0 m.

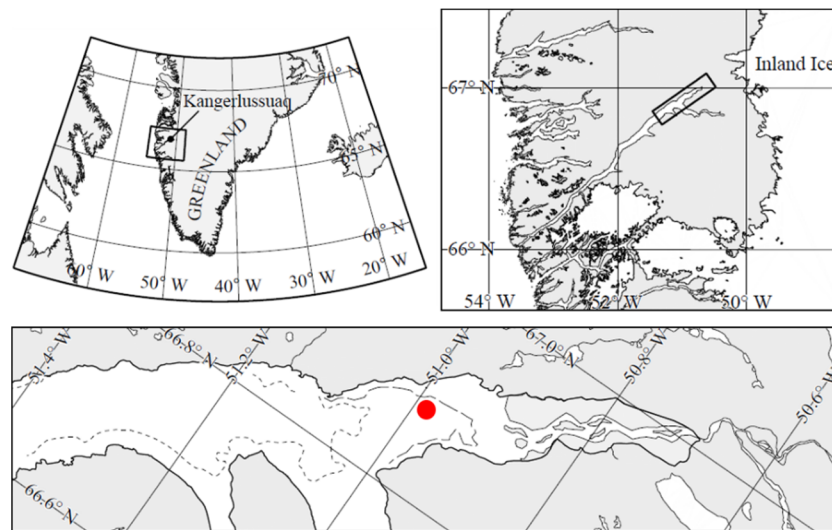


Figure 1. Map showing location of Kangerlussuaq study area in south-west Greenland and location of the sea ice station used in the study (map adopted from Nielsen et al. 2010).

The sea ice station shown in Figure 1 was established on 12 March 2013 (Julian Day 71), at which time a near-uniform ca. 10 mm thick snowpack covered the entire fjord (Figure 2A). High air temperatures and rainfall over Days 74 and 75 caused the entire snow cover of the fjord to melt by Day 75, with the meltwater on the ice preventing access on Days 75 and 76. By Day 77, the warm event had removed all snow from the entire fjord including the study area (Figure 2B).

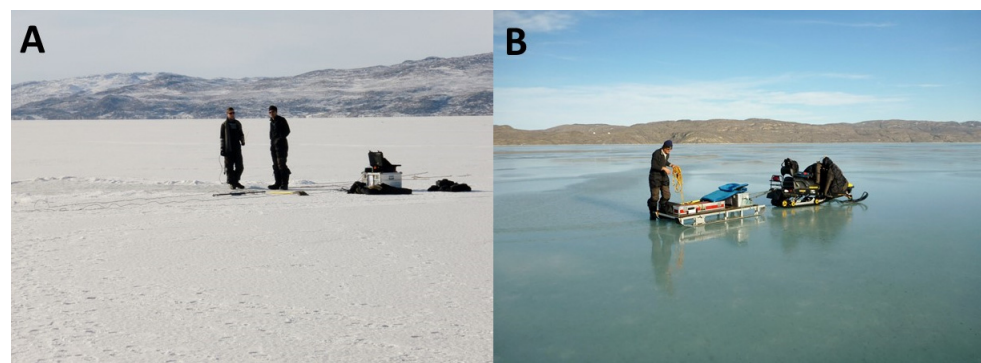


Figure 2. Photos showing change in snow cover on the fjord between (A) Day 71 and (B) Day 77 of the study due to sudden increase in air temperature and rainfall from Days 74–75 (photos by authors).

Sea ice was sampled twice during the cold pre-snowmelt period (Days 71 and 73), which was followed by the melting event (Days 74 to 76), during which the ice station was inaccessible (Figure 3A). After the snowmelt, ice cores were again collected twice (Days 77 and 78). In situ fluorescence imaging was performed on Days 73 (cold, pre-snowmelt) and 78 (warm, post-snowmelt). Sampling was carried out on a 5 m-wide \times 10 m-long sampling area, marked out during the initial establishment of the experiment on Day 71.

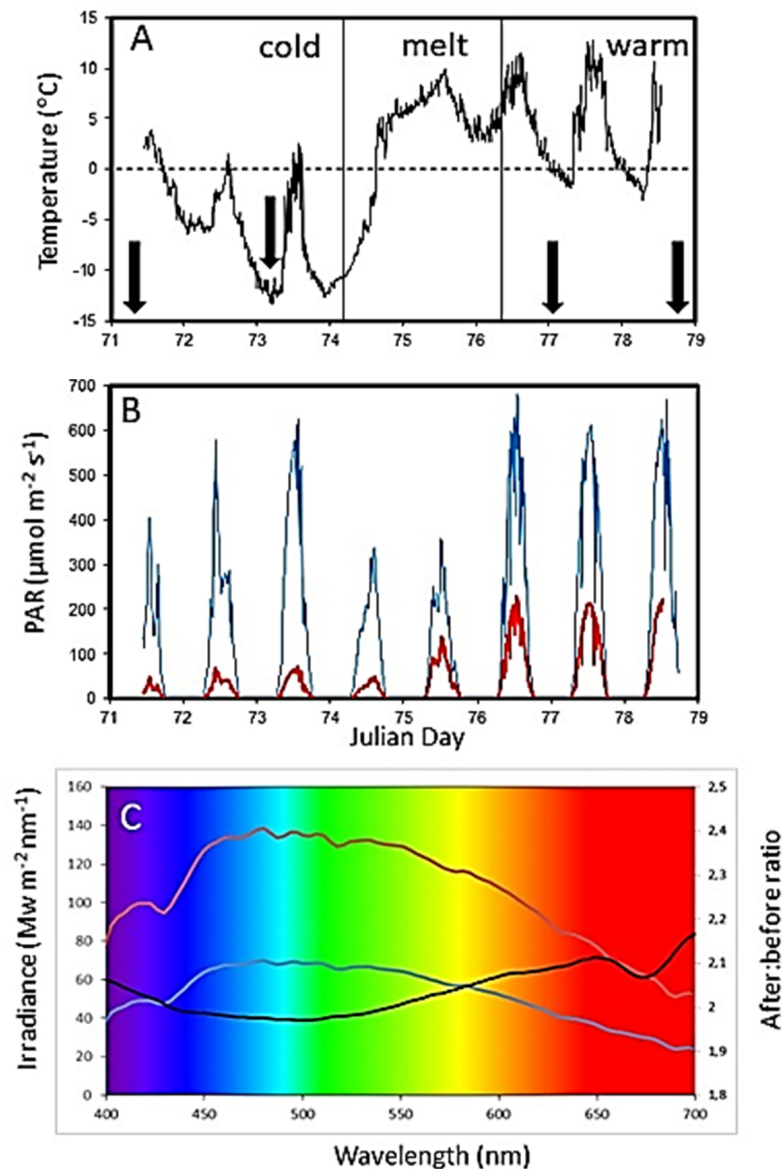


Figure 3. Time series at the sea ice station of (A) air temperature and (B) irradiance (photosynthetically active radiation, PAR) at the ice surface (blue) and under-ice (red). The periods of cold, snow-covered ice, melting snow during the storm event, and post-snowmelt warm ice are shown in (A), with black arrows marking the sampling events (Days 71 and 73 with snow cover, Days 77 and 78 without snow cover). (C) Spectral irradiance under the ice before (blue line) and after (red line) snowmelt. The black line is the ratio of irradiance without:with snow.

2.2. Under-Ice Irradiance

Throughout the experiment, air temperature (sun-screened Campbell 107 temperature probe), downwelling and upwelling photosynthetic photon flux density (PAR) (I_d and I_u) at 0.5 m above the surface (Li-COR Li-191 PAR sensor), and under-ice PAR (I_i) (Li-COR Li-192 submersible PAR sensor) were recorded at the sea ice station at five-minute intervals

using a Campbell CR10X data logger. The under-ice sensor was mounted on a black pole and lowered through a hole in the ice to a measuring position just below the ice and allowed to freeze in place. Transmittance (τ) was calculated as the ratio between under-ice PAR (I_i) and downwelling PAR at the surface (I_d), and albedo was calculated as $[I_u/I_d]$.

To quantify how snow cover affected the spectral distribution of light available to the algae, spectral irradiances were obtained below the ice both with and without snow cover, using a TriOS Ramses ACC VIS cosine-corrected hyperspectral radiometer, measuring from 320 to 950 nm with a 3.3 nm resolution (www.trios.de (accessed on 1 July 2021)). The sensor was mounted on an articulating arm that was lowered through a 90 mm hole in the ice, and once there, the arm unfolded to allow measurements to be obtained just below the ice at a horizontal distance of about 70 cm from the hole. Measurements were taken around local noon with a clear sky.

2.3. Collection, Processing, and Analysis of Ice Cores

Eight ice cores were obtained on each sampling occasion using a 90 mm diameter Kovacs ice corer driven by a battery-powered drill. Their lengths were measured to the nearest 1 mm. Two of the cores were immediately placed in a horizontal cradle and temperature measured to 0.1 °C precision in 3 mm diameter holes drilled every 2.5 cm to the centre of the core. These cores were then cut into 50 mm sections, and each section was sealed in a polyethylene bag and placed in insulated boxes for transportation back to the laboratory within 4 h. The sections were then thawed in individual pots at 4 °C in the dark, and salinity was measured on the thawed sample with a YSI handheld CTD (PRO30) to nearest 0.1 precision. Brine salinity and volume were estimated according to the formulae of Cox and Weeks [28].

Three of the cores from each sampling were used for biological analysis. The lower 30 mm of these cores was removed and immediately used in the field for fluorescence imaging (see next section). The remainder of the core was cut into 50 mm sections. All sections were then sealed in an opaque plastic container to minimise exposure to ambient irradiance and low temperatures and transported to the laboratory. At the laboratory, these biological core sections were placed in individual pots to thaw at 4 °C for ca. 12 h in the dark and to ensure dark adaptation of photosystems before Phyto-PAM analysis (Section 2.5), with an additional two volumes of pre-filtered seawater to prevent osmotic shock [20]. Each sample was immediately subsampled for the Phyto-PAM and filtered as soon as the last visible ice had disappeared, thus ensuring minimum time for any biological degradation or grazing of the algae in the thawed sample. An exact volume of thawed ice (0.25 to 0.5 L) was filtered for estimation of chlorophyll *a* (Chl *a*) through glass fibre filters (GF75 Advantec, nominal pore size 0.7 μ m), using a vacuum of <30 kPa, and the filters packed in aluminium foil and frozen at –20 °C.

Chl *a* was extracted in 5 mL of 96% ethanol at 5 °C for at least 6 h. Samples were centrifuged and the fluorescence of the supernatant measured with a Turner Design fluorometer (TD-700) using excitation of 430 and emission of 665 nm and converted into Chl *a* concentrations using a calibration series of pure pigment.

Three of the non-biological cores were analysed for dissolved organic carbon (DOC), on the lower 30 mm. The lower 30 mm was returned to the laboratory in acid-washed containers for thawing at 4 °C. Subsamples (50 mL) were filtered with a syringe filtration system through pre-combusted (450–500 °C for 2 h) GF/F filters into acid-washed 60 mL HDPE-bottles and preserved by addition of ultrapure 2 N HCl to a final concentration of 0.1%. DOC was later measured using a TOC-VCPH Total Organic Carbon Analyzer (Shimadzu). Deep-water reference Batch 9 Lot # 09/09 (Hansell Laboratory, University of Miami), a four-component freshwater standard series with exactly known C concentration, and freshly produced Milli-Q water as blank were used as reference material. Chl *a* and DOC concentrations were corrected for brine volume.

2.4. In Situ Variable Chlorophyll Fluorescence of Photosystem II—Imaging-PAM

Stress on the photosystems of the sea ice algae from the rapid increase in irradiance after snowmelt was examined through the variable fluorescence of photosystem II (PSII), determined by pulse amplitude modulated (PAM) fluorometry. Variable chlorophyll fluorescence was measured in the field on the intact lower 30 mm section of ice cores using a Walz Imaging-PAM fluorometer. Imaging PAM fluorometry allows resolution of the distribution of pigment systems and the activity of PSII in two dimensions, and full details of methods applied here are given in Hawes et al. [9]. In brief, the instrument was fitted with a lens imaging an area of 30 mm × 24 mm, and the saturation pulse method was used to determine ambient (F) and maximum (F_m') fluorescence yields of samples adapted to under-ice light. From these, we derived the effective quantum yield of PSII (Φ_{PSII}), which is a unitless ratio that is a proxy for the quantum efficiency of photosystem II in electron transfer at the prevailing irradiance; further details are given by Schreiber et al. [29]. We calculated average values of Φ_{PSII} for the entire area of each image obtained as described previously [14].

Our approach was designed to determine Φ_{PSII} in freshly collected ice cores to provide insights into the degree of high-light-induced down-regulation of photosynthesis under the prevailing irradiance regime and to compare this with maximum quantum yield of PSII after overnight dark acclimation ($\Phi_{\text{PSII_max}}$) to discriminate down-regulation from persistent photodamage. Fluorescence imaging was carried out in a darkened tent on the sea ice immediately after sampling in the field. Two types of measurements were made: a single value from triplicate cores collected at local noon on each of Days 73 and 78 and a time course from 09:00 to 17:00 on Day 78. For the time course, each ice core was retained after imaging and thawed overnight (12 h) at 4 °C in the dark as described above for determination of subsequent dark-adapted maximum yield ($\Phi_{\text{PSII_max}}$) using the Phyto-PAM, as described below.

2.5. Variable Chlorophyll Fluorescence of Photosystem II—Phyto-PAM

Triplicate subsamples of the dark-adapted thawed samples as described in Section 2.3 were taken for variable chlorophyll fluorescence estimates in a Phyto-PAM System II Emitter-Detector (Phyto-ED) unit with Phyto-WIN software (www.walz.com.de (accessed on 1 July 2021)), taking care to maintain samples in darkness or very dim light. Measurements of $\Phi_{\text{PSII_max}}$ were performed as described previously [20] on all core sections from the three biological cores. There was no detectable chlorophyll fluorescence in ice sections further up in the core, nor was there any measurable Chl *a* or DOC beyond the lower 30 mm.

In addition, rapid light curves (RLCs) were made for each subsample. RLCs are primarily designed to determine the photophysiological status of cells under a given light regime by exposing cells to short periods of gradually increasing actinic irradiance and measuring Φ_{PSII} by providing a saturation pulse at the end of each irradiance. The product of Φ_{PSII} and actinic irradiance is taken as a measure of electron flow through PSII at that irradiance and referred to as relative electron transfer rate (rETR). From the curves of rETR vs. irradiance, we derived rETR_{max}, the maximum rate of electron flow at light saturation, α , the slope of the light-limited portion of the RLC, and E_k , the irradiance at which rETR was light-saturated, using the algorithms within the Phyto-PAM software. Values of all photobiological parameters for each replicate were the mean of the three subsamples.

2.6. Taxonomic Analysis and Relative Abundance

Samples (100 mL) of thawed bottom ice collected pre-snowmelt on Day 73 and after the snowmelt on Day 77 were preserved with acidic Lugol's solution and stored in the dark for species identification. The ice algae were enumerated according to the Utermöhl method [30]. The samples were allowed to settle in 50 mL settling chambers for 48 h before counting using a Zeiss Axiovert 135M (40×) inverted microscope. A total of four diagonals were counted in each sample. Identification of species and morphological groups

were primarily based on the work by Tomas [31], the relative abundance of algae was estimated as percent of total count, and the algal biomass was calculated according to the ALGESYS protocol.

2.7. Statistical Analysis

All statistical analysis was performed using JASP Version 0.11.1. Differences between sampling dates were compared with repeated-measures ANOVA. *Post hoc* multiple comparisons were conducted with a Bonferroni procedure. The assumption of sphericity was tested with Mauchly's test for all repeated-measures ANOVAs. If violated, the degrees of freedom were corrected using Greenhouse–Geisser estimates of sphericity. For the diel experiment, comparisons were between in situ and dark-acclimated fluorescence yields with time of day as a fixed factor. Data were tested for normality and for heterogeneity of variances with Levene's test and \log_{10} -transformed where necessary.

3. Results

3.1. Physical and Optical Properties

From Days 71 to 73, the air temperature fluctuated between $-12\text{ }^{\circ}\text{C}$ nocturnally and just above freezing point diurnally (Figure 3A). From Day 74 onwards, air temperatures increased rapidly due to the Föhn wind effect and consistently approached or exceeded $+10\text{ }^{\circ}\text{C}$ during the day and rarely fell below the freezing point for the remainder of the study, even at night.

During the cold, snow-covered period, the under-ice light intensity reached a maximum value of $56\text{ }\mu\text{mol photons m}^{-2}\text{ s}^{-1}$ at noon on Day 73, with an average albedo of 0.64 and transmittance of 0.33 (Figure 3B). After the melting of snow and warming of the ice, PAR albedo decreased to 0.21, transmittance increased to 0.48, and under-ice irradiances were as high as $183\text{ }\mu\text{mol photons m}^{-2}\text{ s}^{-1}$ on Day 76, four times higher than prior to snowmelt despite similar incident irradiance at the surface of the sea ice. Spectral composition was dominated by blue-green wavelengths, with maximum transmittance close to 480 nm but with a higher absorption in the red part of the spectrum with snow cover, consistent with how peak irradiance absorption by snow occurs at ca. 670 nm (Figure 3C).

3.2. Effect of the Snowmelt on Sea Ice Temperature and Brine Volume

The ice thickness was uniform at the field station, being $0.74 \pm 0.01\text{ m}$ ($n = 4$ cores) before snowmelt, and identical ($0.74 \pm 0.01\text{ m}$, $n = 8$) after snowmelt. On Day 73, the ice temperature profile showed a surface ice temperature of $-6\text{ }^{\circ}\text{C}$, rising to $-1.8\text{ }^{\circ}\text{C}$ at the ice–water interface (Figure 4A). Subsequently, during the snowmelt event, the ice became almost isothermal and at the ice–water interface was $-1.4\text{ }^{\circ}\text{C}$. Brine volume increased with the warming of the ice over this time, with the increase in volume greatest in the upper part of the ice column (Figure 4B).

3.3. Chl *a* and DOC Concentrations

The snowmelt event had significant effects on Chl *a* concentrations and DOC in the lower 30 mm of the ice (Table 1). Before the snowmelt, Chl *a* and DOC did not differ significantly between Days 71 and 73. Chl *a* then decreased approximately two-fold under snow-free conditions in response to the melting event. The decrease in DOC was similar in magnitude to that of Chl *a*.

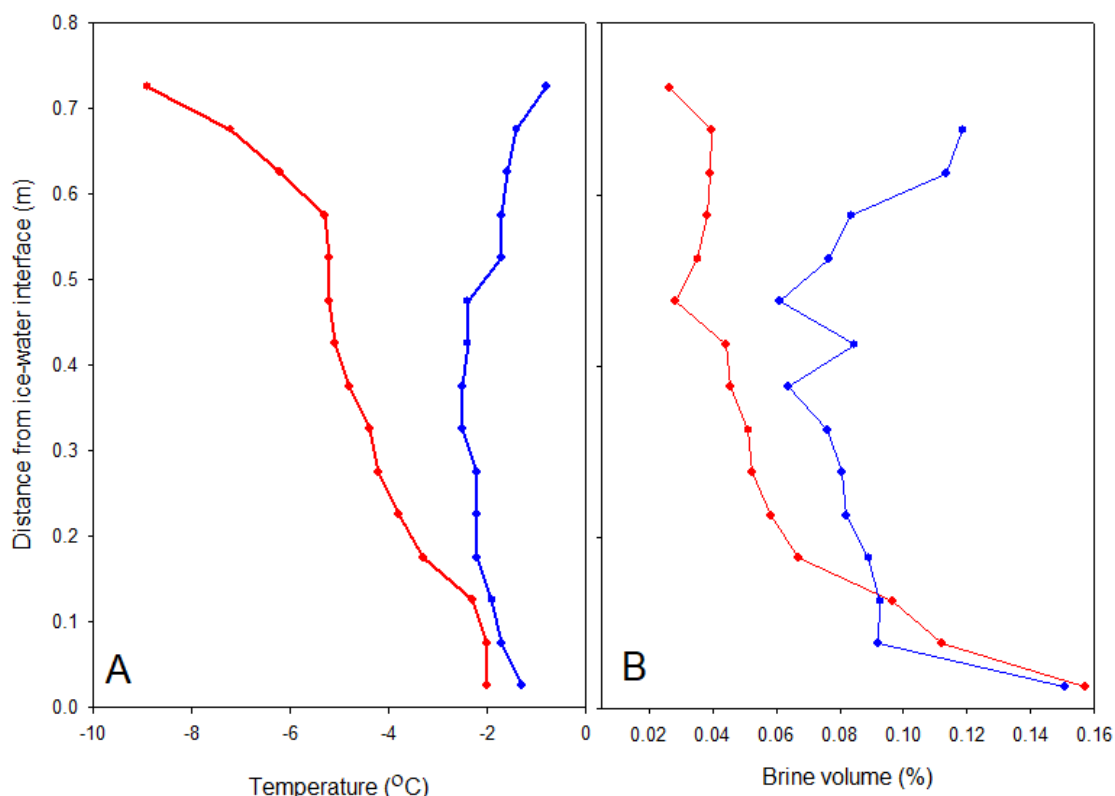


Figure 4. Ice temperature (A) and brine volume (B) profiles during the cold (pre-snowmelt, Day 73, red line) and warm (post-snowmelt, Day 77, blue line) phases of the experiment. Values are means at each depth from two cores.

Table 1. Mean \pm SD ($n = 3$) for Chl *a*, DOC (dissolved organic carbon), Φ_{PSII_max} , α , $rETR_{max}$, and E_k for the lower 30 mm of the ice before (Days 71 and 73) and after (Days 77 and 79) snowmelt on the fjord. *F* values from repeated-measures ANOVA shown with significant tests identified as $p < 0.05$ *, $p < 0.01$ **. Different letter superscripts within rows identify means that differ significantly where ANOVA is significant. Chl *a* and DOC were sampled on all four occasions; photobiology (Phyto-PAM) was not performed on Day 71 (n.d. = not determined). Degrees of freedom are 3, 9 for Chl *a* and DOC, and 2, 6 for photobiology.

	Day 71	Day 73	Day 77	Day 78	<i>F</i>
Chl <i>a</i> (mg m ⁻²)	^a 1.75 \pm 1.11	^a 0.85 \pm 0.13	^b 0.35 \pm 0.08	^b 0.37 \pm 0.05	33.87 **
DOC (μ mol L ⁻¹)	^a 100 \pm 33	^a 122 \pm 35	^b 60 \pm 8	^b 59 \pm 6	9.63 *
Φ_{PSII_max}	n.d.	^a 0.55 \pm 0.03	^b 0.40 \pm 0.03	^b 0.41 \pm 0.05	15.90 **
α (mol ϵ mol ⁻¹ photons)	n.d.	^a 0.22 \pm 0.01	^b 0.16 \pm 0.01	^b 0.17 \pm 0.02	10.71 *
$rETR_{max}$ (μ mol ϵ m ⁻² s ⁻¹)	n.d.	10.6 \pm 3.9	8.3 \pm 3.2	5.3 \pm 1.0	1.89
E_k (μ mol photon m ⁻² s ⁻¹)	n.d.	49 \pm 19	54 \pm 22	33 \pm 10	0.87

3.4. Variable Chlorophyll Fluorescence

Table 1 shows that some ice algae photosynthetic parameters in the lower 30 mm of the ice also changed significantly following loss of snow cover. After overnight dark adaptation of thawed samples, Φ_{PSII_max} measured by Phyto-PAM analysis was significantly lower in post-snowmelt samples than pre-snowmelt samples, and α also declined, while E_k and $rETR_{max}$ did not change significantly.

Comparison of fluorescence (*F*) images of the underside of the bottom sections, obtained immediately on collection of ice cores in the field, also showed distinct differences before and after snowmelt. Prior to the loss of snow cover, *F* images show algae organized in distinct aggregates, associated with the tops of ridges in the crystalline ice matrix (Figure 5A). These parallel elongated structures of high *F* in the snow-covered ice occur

where ice algae are attached to the ice crystals, which develop a dendritic structure at the bottom of the ice. In contrast, there were fewer and less organized algal aggregates and visibly lower F after snowmelt (Figure 5B). Data from analysis of images of ice collected at local noon ($n = 3$ cores) showed $F = 0.071 \pm 0.005$ before snowmelt, falling to $F = 0.023 \pm 0.002$ after snowmelt. This decrease in F between the cold and warm periods parallels the decrease in Chl a (Table 1).

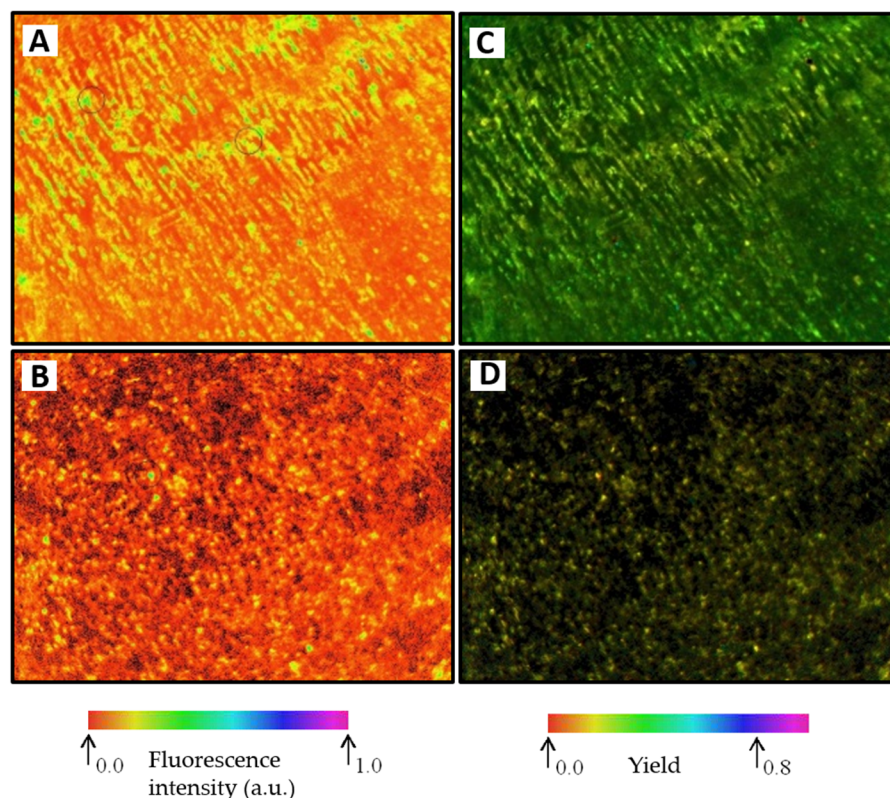


Figure 5. Examples of in situ fluorescence images of F (A,B) and Φ_{PSII_max} (C,D), comparing chlorophyll distribution and activity from base of ice cores on Day 73 before snowmelt (A,C) and Day 78 after snowmelt (B,D). The false colours indicate relative fluorescence intensity of F and Φ_{PSII_max} as per the corresponding scales, and all images were taken at the same instrument measuring light and gain settings. All images are 30×23 mm.

There was also a clear reduction in the operational quantum yield (Φ_{PSII}) at local noon, comparing the pre-snowmelt community (Figure 5C) to post-snowmelt cores (Figure 5D). Image analysis ($n = 3$ cores) gave $\Phi_{PSII} = 0.36 \pm 0.02$ before snowmelt, falling to 0.12 ± 0.01 after snowmelt.

3.5. Diel Photobiology and Dark Recovery (Day 78)

The mean value of Φ_{PSII_max} was 0.52 before sunrise and showed a circadian rhythm, decreasing in the middle of the day, before rising in the evening. Φ_{PSII} was similar to Φ_{PSII_max} before dawn. By local noon, cells showed a down-regulation of photosynthesis, with Φ_{PSII} falling to 0.20 ± 0.01 from pre-dawn (06:00) values of 0.45 ± 0.03 . The diel cycle of Φ_{PSII} (Figure 6) followed the in situ irradiance. Following overnight dark adaptation, there was effective recovery to near pre-illuminated values in all samples.

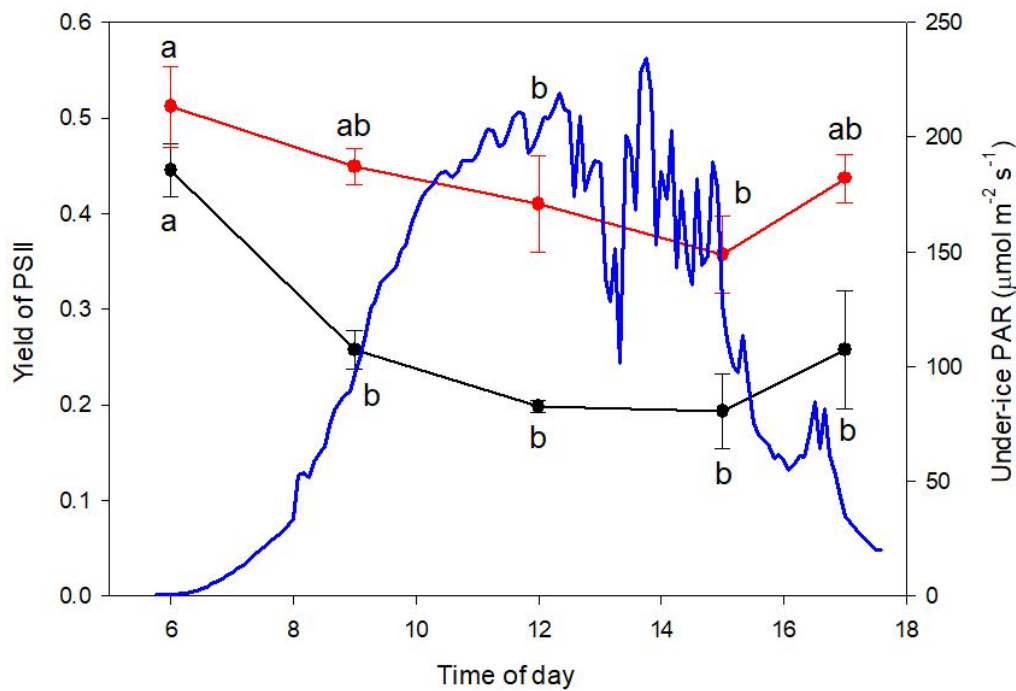


Figure 6. Diel cycles in yield of PSII for sea ice algae on Day 78 after loss of snow cover on fjord. Black line shows Φ_{PSII} measured immediately after collection by Imaging-PAM fluorometry, red line shows $\Phi_{\text{PSII_max}}$ after subsequent thawing in dark measured by Phyto-PAM fluorometry. Mean values \pm 1SD, $n = 3$. Significant differences between time points at $p < 0.05$ (repeated-measures ANOVA, *post hoc* Bonferroni tests) shown for each curve by different letters adjacent to symbols. Blue line shows continuous monitoring of irradiance as photosynthetically active radiation (PAR) immediately under ice.

3.6. Ice Algae Cell Numbers, Species Composition, and Relative Abundance

There was no significant difference in total algal abundance ($t = 1.78$, $p = 0.15$) before ($18,250 \pm 5992$ cells L^{-1}) and after ($21,797 \pm 4164$ cells L^{-1}) the snowmelt, but the species composition changed. In the pre-snowmelt samples (Day 73) diatoms ($38 \pm 10\%$) and small, unidentified flagellates ($55 \pm 7\%$) dominated species composition. After snowmelt (Day 77), both were still present, but the proportion of diatoms had increased to $67 \pm 19\%$, whereas relative abundance of flagellates nearly halved to $23 \pm 13\%$. Despite the change in species composition, the total algal biomass was unchanged, from 1468 ± 923 $\mu\text{gC L}^{-1}$ before snowmelt to 1756 ± 896 $\mu\text{gC L}^{-1}$ after snowmelt.

The pennate diatoms *Nitzschia closterium*, *N. longissima*, and *N. frigida* were common in all ice algal samples, both before and after snowmelt. The chain-forming pennate *Fragilaria* sp. and the centric *Thalassiosira* spp. were also common under snow cover but largely disappeared from the community after snowmelt. *Nitzschia frigida* was the only taxon to significantly increase its relative abundance after the melting event, when it became the dominant species.

4. Discussion

Snow-clearing experiments are commonly used for investigating effects of snowmelt on polar sea ice algae [12,14,32]. The fortuitous weather event documented in this paper has allowed us to explore how the results of such experiments compare against a natural snow loss event featuring a 17 $^{\circ}\text{C}$ atmospheric warming. In contrast to snow-clearing experiments in which air temperature remains unchanged, the main effect apart from increased irradiance is removal of the insulating effect of snow. Exposure to warmer air temperatures may lead to increased brine volume and potentially brine drainage and ultimately heat loss and melting of the sea ice. The general findings of snow-clearing experiments are that sudden increases in irradiance when snow is cleared cause rapid loss of shade-adapted taxa, leading to immediately lower sea ice algal biomass, and subsequent

increases in taxa tolerant of higher irradiances [12,14,20]. A similar response was seen here in the overall response of Kangerlussuaq Fjord to wholesale snow loss, suggesting that these large weather events produce similar effects to smaller-scale snow-clearing experiments.

Snow loss can lead to reduced sea ice algal biomass through both physical mechanisms and photobiological effects. Snow is a very effective thermal insulator, protecting sea ice from atmospheric temperature fluctuations. Loss of snow cover increases thermal exchange between ice and atmosphere; in this case, the sudden atmospheric warming increased heat transfer into the ice, leading to melting and loss of the millimetre-thin crystalline skeletal layer on the underside of the ice. A large fraction of the ice algal biomass is often associated with this crystalline layer [8] as it provides a large surface area for colonisation, especially when actively growing [33]. Documenting developments in the structure of the underside of the ice and its relation to biomass and photobiology is one of the benefits of the Imaging-PAM method. With this method, we were able in this study to observe the loss of the crystalline structure and replacement of its well-organised ice algal aggregates with a poorly defined ice surface and much smaller clumps of algae. Comparing the F and $\Phi_{\text{PSII}_{\text{max}}}$ images before and after snow loss illustrates the change in distribution and activity caused by the cold–warm event and confirms physical ablation of the skeletal layer as an important mechanism in the algal loss observed here. The corresponding decrease in Chl *a* content and DOC confirms a substantial change in the community after snow loss. Brine drainage is an additional physical mechanism that can lead to loss of ice algae when air temperatures warm the ice and increase brine permeability. However, this mechanism was unlikely to be important for the measured photophysiological variables in the current study as all of the algae before the snowmelt were associated with the crystals of the skeletal brine layer in the lowest 10–15 mm, as seen in the fluorescence images (Figure 5).

PAM fluorometric techniques are also valuable in establishing the extent of photoinhibition stress suffered by the ice algal community and its role in ice algal loss. Rapid changes from low to high irradiance cause photoinhibition in sea ice algae because they are characteristically extremely shade-adapted organisms [1] and photoacclimate to the very low irradiances under snow-covered sea ice [32,34]. $\Phi_{\text{PSII}_{\text{max}}}$ is now well-established as an extremely sensitive indicator of photoinhibition that often responds rapidly and before any observable loss of biomass [20,35]. Here, as also seen in snow-clearing experiments [20], its decrease immediately when the snow disappeared confirms the rapid onset of photoinhibition in the community. It is important, when interpreting these data, to note that the photobiological data from Day 77 after the snowmelt represents those algae that persisted or colonised in spite of increased irradiance. The flagellates and diatoms lost between Days 73 and 77 were either physically lost, killed by excess photostress, or migrated out of the ice. The remaining community—dominated especially by *N. frigida*—is able to remain active and grow despite the photoinhibition evident from the lower $\Phi_{\text{PSII}_{\text{max}}}$. In particular, $r\text{ETR}_{\text{max}}$ was not significantly lower in the post-snowmelt community, confirming that high-light-tolerant taxa remained active and may even have grown in the increased irradiance. The fact that the algal cell numbers and carbon content of the lower 30 mm did not change after the snowmelt even though Chl *a* decreased suggests that the post-snowmelt community consisted of cells with a lower Chl *a* content, due either to the change in taxonomic composition or acclimation by the pre-snowmelt taxa that persisted after snow loss. The contribution of *N. frigida* is particularly interesting here. *N. frigida* is known as a sea-ice specialist [12,36] and well-established as highly shade-tolerant species [37]. Our study suggests that its adaptation to the sea ice habitat comes not only from being shade-adapted but also from an ability to tolerate higher light intensities and be robust in response to the rapid light fluctuations that are a feature of sea ice.

In this study, we applied two PAM fluorescence methods that provided complementary information on the nature of photoinhibition in the community after snowmelt. Imaging-PAM data measured in the field immediately after collection of cores illustrated the operational fluorescence yield Φ_{PSII} under the prevailing PAR at the time of collection, whereas Phyto-PAM data measured after thawing of core slices provided $\Phi_{\text{PSII}_{\text{max}}}$ after

all reaction centres had had more than 12 h to relax in the dark in optimal conditions. The Imaging-PAM Φ_{PSII} data show a typical diurnal cycle of yield associated with photosynthetic activity and non-photosynthetic quenching with the diatinoxanthin–diadinoxanthin cycle. The post-snowmelt community was not showing any signs of photodamage, given that Φ_{PSII} before sunrise at 06:00 h in the fresh cores was not significantly lower than in the same cores after thawing overnight for the Phyto-PAM. Some non-photosynthetic quenching associated with energy dissipation is implied by the diurnal cycle in $\Phi_{\text{PSII_max}}$ observed in the Phyto-PAM, but there is apparently not any severe photodamage, and it is likely that the community would continue to acclimate to the higher irradiance as the higher irradiance persisted. There was also no indication of any decline in rETR at higher irradiances that would indicate photodamage. We have previously observed recovery of $\Phi_{\text{PSII_max}}$ and other photobiological parameters at this site after an initial decrease, in conjunction with colonisation of larger, higher-light taxa [14,20]. This is also a typical feature of the seasonal development of the ice algal community during a spring bloom in landfast seasonal ice, where early-season flagellates and small taxa are gradually replaced by the pennate diatom community [22], climaxing in the larger taxa that are most high-light-tolerant [38], before summer snowmelt.

This study, along with the snow-clearing experiments it can be compared and contrasted with, confirms the prime importance of snow cover as the predominant factor controlling the composition, timing, and productivity of the ice algal community [39]. Comparing against two other studies from the same site and the same time of year (March, spring bloom) in 2011 [14] and 2016 [20], both the pre-snowmelt/snow-clearing and post-snow-removal communities were different. In 2011, under ca. 8 cm snow, the pre-bloom community was dominated by *Fragillariopsis oceanica*, which was the main species lost after snow removal [14]. *F. oceanica* was rare or absent at all times in the current study, whereas *N. frigida* was rare in 2011 both before and after snow loss/removal. In 2016, flagellates were rare to begin with, but *N. frigida* and other *Nitzschia* spp. increased after snow removal. Light history can certainly explain these taxonomic differences: in both of those years, the under-ice irradiance was considerably lower than the ca. 60 $\mu\text{mol photons m}^{-2} \text{s}^{-1}$ in 2013. Early-season communities dominated by small diatoms and flagellates can photosynthesise and grow at light intensities $<10 \mu\text{mol photons m}^{-2} \text{s}^{-1}$ [32,40]. The inter-annual variability at this site, despite having a very uniform landfast ice structure and similar water temperature and unlimited nutrient availability at the time of the spring bloom, is testimony to how small differences in snow cover can have dramatic effects on the ice algal community. Although snow thickness is important, the high albedo of snow is its main property giving a high light attenuation, and thus presence or absence of snow cover is particularly important. In the present study, we can see a dramatic change when even a very thin snow cover is removed. Predicting the future of sea ice communities is therefore challenging, given the increasing frequency of wind and warming events with climate change, but one robust conclusion is that disruption of the normal progress of the spring bloom is likely to become more common. On the other hand, the results of this study and others suggest that some ice algal taxa, although briefly stressed when snow disappears, are capable of acclimating and recovering and continuing production even under greatly increased irradiances.

In conclusion, by documenting algal biomass, species composition, and photobiological responses to this whole-fjord snow loss event, we observed similar responses to artificial snow clearance. Photobiological effects of changes in irradiance appear to remain central to these effects, irrespective of the scale or cause of snow loss. Finally, we provided additional information here on the photobiological properties of first-year sea ice algae, which are highly dynamic features of the community. Many models exist that relate Chl *a* to snow depth and ice thickness [23,39], but only recently have models begun to include photobiological parameters [24]. Snow-clearing experiments, particularly longer-term experiments that allow both photostress but also include time for recovery, will remain an important tool for exploring the future of sea ice ecosystems.

Author Contributions: Conceptualization, L.C.L.-H. and B.K.S.; all authors contributed in the collection of field data; L.C.L.-H. performed light attenuation and brine volume calculations; I.H. performed the fluorescence imaging; B.K.S. performed statistical analyses and created the plots; all authors contributed to the writing of the article. All authors have read and agreed to the published version of the manuscript.

Funding: This project was funded by the Danish Council for Independent Research (Project DFF-1323-00335: Sea ice ecosystems: Ecological effects of a thinning snow cover), the New Zealand Ministry of Business, Innovation and Employment (Project ANTA1801), the Carlsberg Foundation, Aarhus University, and the Hartmann Brothers Foundation and was developed in the frame of the project FACE-IT (The Future of Arctic Coastal Ecosystems—Identifying Transitions in Fjord Systems and Adjacent Coastal Areas). FACE-IT has received funding from the European Union’s Horizon 2020 research and innovation program under grant agreement No. 869154.

Institutional Review Board Statement: Not applicable.

Informed Consent Statement: Not applicable.

Data Availability Statement: Data are available from authors pending reasonable requests.

Acknowledgments: We thank the staff at Kangerlussuaq International Science Support (KISS) for logistical help and assistance. We thank Per Andersen for species identifications and Ida Marie Deichmann for laboratory assistance.

Conflicts of Interest: The authors declare no conflict of interest.

References

- Selz, V.; Laney, S.; Arnsten, A.E.; Lewis, K.M.; Lowry, K.E.; Joy-Warren, H.L.; Mills, M.M.; van Dijken, G.L.; Arrigo, K.R. Ice algal communities in the Chukchi and Beaufort Seas in spring and early summer: Composition, distribution, and coupling with phytoplankton assemblages. *Limnol. Oceanogr.* **2018**, *63*, 1109–1133. [\[CrossRef\]](#)
- Fernández-Méndez, M.; Wenzhöfer, F.; Peeken, I.; Sørensen, H.L.; Glud, R.N.; Boetius, A. Composition, buoyancy regulation and fate of ice algal aggregates in the Central Arctic Ocean. *PLoS ONE* **2014**, *9*, e107452. [\[CrossRef\]](#)
- Kohlbach, D.; Lange, B.A.; Schaafsma, F.L.; David, C.; Vortkamp, M.; Graeve, M.; van Franeker, J.A.; Krumpfen, T.; Flores, H. Ice algae-produced carbon is critical for overwintering of antarctic krill *Euphausia superba*. *Front. Mar. Sci.* **2017**, *4*, 1–16. [\[CrossRef\]](#)
- Castellani, G.; Schaafsma, F.L.; Arndt, S.; Lange, B.A.; Peeken, I.; Ehrlich, J.; David, C.; Ricker, R.; Krumpfen, T.; Hendricks, S.; et al. Large-scale variability of physical and biological sea-ice properties in polar oceans. *Front. Mar. Sci.* **2020**, *7*, 1–22. [\[CrossRef\]](#)
- Brown, T.A.; Galicia, M.P.; Thiemann, G.W.; Belt, S.T.; Yurkowski, D.J.; Dyck, M.G. High contributions of sea ice derived carbon in polar bear (*Ursus maritimus*) tissue. *PLoS ONE* **2018**, *13*, 1–13. [\[CrossRef\]](#)
- Arrigo, K.R.; van Dijken, G.; Pabi, S. Impact of a shrinking Arctic ice cover on marine primary production. *Geophys. Res. Lett.* **2008**, *35*, 1–6. [\[CrossRef\]](#)
- Lund-Hansen, L.C.; Bendtsen, J.; Stratmann, T.; Tonboe, R.; Olsen, S.M.; Markager, S.; Sorrell, B.K. Will low primary production rates in the Amundsen Basin (Arctic Ocean) remain low in a future ice-free setting, and what governs this production? *J. Mar. Syst.* **2020**, *205*, 103287. [\[CrossRef\]](#)
- McMinn, A.; Martin, A.; Ryan, K. Phytoplankton and sea ice algal biomass and physiology during the transition between winter and spring (McMurdo Sound, Antarctica). *Polar Biol.* **2010**, *33*, 1547–1556. [\[CrossRef\]](#)
- Hawes, I.; Lund-Hansen, L.C.; Sorrell, B.K.; Nielsen, M.H.; Borzák, R.; Buss, I. Photobiology of sea ice algae during initial spring growth in Kangerlussuaq, West Greenland: Insights from imaging variable chlorophyll fluorescence of ice cores. *Photosynth. Res.* **2012**, *112*, 103–115. [\[CrossRef\]](#) [\[PubMed\]](#)
- Olsen, L.M.; Laney, S.R.; Duarte, P.; Kauko, H.M.; Fernández-Méndez, M.; Mundy, C.J.; Rösel, A.; Meyer, A.; Itkin, P.; Cohen, L.; et al. The seeding of ice algal blooms in Arctic pack ice: The multiyear ice seed repository hypothesis. *J. Geophys. Res. Biogeosci.* **2017**, *122*, 1529–1548. [\[CrossRef\]](#)
- Gradinger, R.; Bluhm, B. Timing of ice algal grazing by the Arctic nearshore benthic amphipod *Onisimus litoralis*. *Arctic* **2010**, *63*, 355–358. [\[CrossRef\]](#)
- Juhl, A.R.; Krembs, C. Effects of snow removal and algal photoacclimation on growth and export of ice algae. *Polar Biol.* **2010**, *33*, 1057–1065. [\[CrossRef\]](#)
- Mundy, C.J.; Barber, D.G.; Michel, C. Variability of snow and ice thermal, physical and optical properties pertinent to sea ice algae biomass during spring. *J. Mar. Syst.* **2005**, *58*, 107–120. [\[CrossRef\]](#)
- Lund-Hansen, L.C.; Hawes, I.; Sorrell, B.K.; Nielsen, M.H. Removal of snow cover inhibits spring growth of Arctic ice algae through physiological and behavioral effects. *Polar Biol.* **2014**, *37*, 471–481. [\[CrossRef\]](#)
- Callaghan, T.V.; Johansson, M.; Brown, R.D.; Groisman, P.Y.; Labba, N.; Radionov, V.; Barry, R.G.; Bulygina, O.N.; Essery, R.L.H.; Frolov, D.M.; et al. The changing face of Arctic snow cover: A synthesis of observed and projected changes. *Ambio* **2011**, *40*, 17–31. [\[CrossRef\]](#)

16. Bintanja, R.; Andry, O. Towards a rain-dominated Arctic. *Nat. Clim. Chang.* **2017**, *7*, 263–267. [[CrossRef](#)]
17. Warren, S.G.; Rigor, I.G.; Untersteiner, N.; Radionov, V.F.; Bryazgin, N.N.; Aleksandrov, Y.I.; Colony, R. Snow depth on Arctic sea ice. *J. Clim.* **1999**, *12*, 1814–1829. [[CrossRef](#)]
18. Kwok, R.; Cunningham, G.F.; Wensnahan, M.; Rigor, I.; Zwally, H.J.; Yi, D. Thinning and volume loss of the Arctic Ocean sea ice cover: 2003–2008. *J. Geophys. Res. Ocean.* **2009**, *114*, 2003–2008. [[CrossRef](#)]
19. Santolaria-Otín, M.; Zolina, O. Evaluation of snow cover and snow water equivalent in the continental Arctic in CMIP5 models. *Clim. Dyn.* **2020**, *55*, 2993–3016. [[CrossRef](#)]
20. Lund-Hansen, L.C.; Hawes, I.; Hancke, K.; Salmansen, N.; Nielsen, J.R.; Balslev, L.; Sorrell, B.K. Effects of increased irradiance on biomass, photobiology, nutritional quality, and pigment composition of Arctic sea ice algae. *Mar. Ecol. Prog. Ser.* **2020**, *648*, 95–110. [[CrossRef](#)]
21. Manes, S.S.; Gradinger, R. Small scale vertical gradients of Arctic ice algal photophysiological properties. *Photosynth. Res.* **2009**, *102*, 53–66. [[CrossRef](#)] [[PubMed](#)]
22. Leu, E.; Mundy, C.J.; Assmy, P.; Campbell, K.; Gabrielsen, T.M.; Gosselin, M.; Juul-Pedersen, T.; Gradinger, R. Arctic spring awakening—Steering principles behind the phenology of vernal ice algal blooms. *Prog. Oceanogr.* **2015**, *139*, 151–170. [[CrossRef](#)]
23. Campbell, K.; Mundy, C.J.; Barber, D.G.; Gosselin, M. Characterizing the sea ice algae chlorophyll a-snow depth relationship over Arctic spring melt using transmitted irradiance. *J. Mar. Syst.* **2015**, *147*, 76–84. [[CrossRef](#)]
24. Sibert, V.; Zakardjian, B.; Saucier, F.; Gosselin, M.; Starr, M.; Senneville, S. Spatial and temporal variability of ice algal production in a 3D ice-ocean model of the Hudson Bay, Hudson Strait and Foxe Basin system. *Polar Res.* **2010**, *29*, 353–378. [[CrossRef](#)]
25. Yoshida, K.; Seger, A.; Corkill, M.; Heil, P.; Karsh, K.; McMinn, A.; Suzuki, K. Low Fe availability for photosynthesis of sea-ice algae: Ex situ incubation of the ice diatom *Fragilariopsis cylindrus* in low-Fe sea ice using an ice tank. *Front. Mar. Sci.* **2021**, *8*, 1–20. [[CrossRef](#)]
26. Lund-Hansen, L.C.; Andersen, T.J.; Nielsen, M.H.; Pejrup, M. Suspended matter, Chl-*a*, CDOM, grain sizes, and optical properties in the Arctic fjord-type estuary, Kangerlussuaq, West Greenland during summer. *Estuaries Coasts* **2010**, *33*, 1442–1451. [[CrossRef](#)]
27. Nielsen, M.H.; Erbs-Hansen, D.R.; Knudsen, K.L. Water masses in Kangerlussuaq, a large fjord in West Greenland: The processes of formation and the associated foraminiferal fauna. *Polar Res.* **2010**, *29*, 159–175. [[CrossRef](#)]
28. Cox, G.F.N.; Weeks, W.F. Equations for determining the gas and brine volumes in sea ice samples. *J. Glaciol.* **1983**, *29*, 306–316. [[CrossRef](#)]
29. Schreiber, U.; Hormann, H.; Neubauer, C.; Klughammer, C. Assessment of Photosystem II photochemical quantum yield by chlorophyll fluorescence quenching analysis. *Funct. Plant Biol.* **1995**, *22*, 209. [[CrossRef](#)]
30. Utermöhl, H. Zur Vervollkommnung der quantitativen Phytoplankton-Methodik. *SIL Commun.* 1953–1996 **1958**, *9*, 1–38. [[CrossRef](#)]
31. Tomas, C.R. *Identifying Marine Phytoplankton*; Academic Press: San Diego, CA, USA, 1997.
32. Hancke, K.; Lund-Hansen, L.C.; Lamare, M.L.; Højlund Pedersen, S.; King, M.D.; Andersen, P.; Sorrell, B.K. Extreme low light requirement for algae growth underneath sea ice: A case study from Station Nord, NE Greenland. *J. Geophys. Res. Ocean.* **2018**, *123*, 985–1000. [[CrossRef](#)]
33. Lund-Hansen, L.C.; Hawes, I.; Nielsen, M.H.; Sorrell, B.K. Is colonization of sea ice by diatoms facilitated by increased surface roughness in growing ice crystals? *Polar Biol.* **2017**, *40*, 593–602. [[CrossRef](#)]
34. Galindo, V.; Gosselin, M.; Lavaud, J.; Mundy, C.J.; Else, B.; Ehn, J.; Babin, M.; Rysgaard, S. Pigment composition and photoprotection of Arctic sea ice algae during spring. *Mar. Ecol. Prog. Ser.* **2017**, *585*, 49–69. [[CrossRef](#)]
35. Yoshida, K.; Seger, A.; Kennedy, F.; McMinn, A.; Suzuki, K. Freezing, melting, and light stress on the photophysiology of ice algae: Ex situ incubation of the ice algal diatom *Fragilariopsis cylindrus* (Bacillariophyceae) using an ice tank. *J. Phycol.* **2020**, *56*, 1323–1338. [[CrossRef](#)] [[PubMed](#)]
36. Aumack, C.F.; Juhl, A.R. Light and nutrient effects on the settling characteristics of the sea ice diatom *Nitzschia frigida*. *Limnol. Oceanogr.* **2015**, *60*, 765–776. [[CrossRef](#)]
37. Croteau, D.; Guérin, S.; Bruyant, F.; Ferland, J.; Campbell, D.A.; Babin, M.; Lavaud, J. Contrasting nonphotochemical quenching patterns under high light and darkness aligns with light niche occupancy in Arctic diatoms. *Limnol. Oceanogr.* **2021**, *66*, S231–S245. [[CrossRef](#)]
38. Kauko, H.M.; Olsen, L.M.; Duarte, P.; Peeken, I.; Granskog, M.A.; Johnsen, G.; Fernández-Méndez, M.; Pavlov, A.K.; Mundy, C.J.; Assmy, P. Algal colonization of young arctic sea ice in spring. *Front. Mar. Sci.* **2018**, *5*, 199. [[CrossRef](#)]
39. Lange, B.A.; Haas, C.; Charette, J.; Katlein, C.; Campbell, K.; Duerksen, S.; Coupel, P.; Anhaus, P.; Jutila, A.; Tremblay, P.O.G.; et al. Contrasting ice algae and snow-dependent irradiance relationships between first-year and multiyear sea ice. *Geophys. Res. Lett.* **2019**, *46*, 10834–10843. [[CrossRef](#)]
40. Mock, T.; Gradinger, R. Changes in photosynthetic carbon allocation in algal assemblages of Arctic sea ice with decreasing nutrient concentrations and irradiance. *Mar. Ecol. Prog. Ser.* **2000**, *202*, 1–11. [[CrossRef](#)]